

# Generation of Fock-State Superpositions and Binomial-Code Holonomic Gates via Dressed Intermediate States in the Ultrastrong Light-Matter Coupling Regime

Ye-Hong Chen,<sup>1</sup> Wei Qin,<sup>1</sup> Roberto Stassi,<sup>1, 2</sup> Xin Wang,<sup>1, 3</sup> and Franco Nori<sup>1, 4</sup>

<sup>1</sup> Theoretical Quantum Physics Laboratory, RIKEN Cluster for Pioneering Research, Wako-shi, Saitama 351-0198, Japan

<sup>2</sup> Dipartimento di Scienze Matematiche e Informatiche,

Scienze Fisiche e Scienze della Terra, Università di Messina, 98166, Messina, Italy

<sup>3</sup> Institute of Quantum Optics and Quantum Information,

School of Science, Xi'an Jiaotong University, Xi'an 710049, China

<sup>4</sup> Department of Physics, University of Michigan, Ann Arbor, Michigan 48109-1040, USA

(Dated: November 4, 2021)

By using the dressed-state properties of an ultrastrong coupling system, we propose to generate and manipulate, with high fidelities, arbitrary superposition of Fock states. These generated states can form bosonic codes (e.g., binomial codes) to implement nonadiabatic holonomic quantum computation, making the computation *fast, robust, and fault-tolerant*. The holonomic gates are induced by *geometric phases*, which possess a built-in noise-resilience feature against local noises. No high-order processes or nonlinear drivings are needed in this work, so that the quantum gates can be implemented in *tens of nanoseconds*. Such a fast evolution makes our protocols robust against decoherence caused by the decays and dephasings of both the cavity and the atom. Moreover, we design the control fields by a systematic-error-sensitivity nullification method, thus our protocols can be mostly insensitive to systematic errors caused by pulse imperfections.

Keywords: Nonadiabatic holonomic quantum computation; Bosonic code; Shortcuts to adiabaticity

*Introduction.*—The generation of robust and fault-tolerant quantum gates is a basic requirement for quantum computation. To this goal, much attention has been given to holonomic quantum computation [1–4] based on Abelian [5, 6] and non-Abelian geometric phases [7–9]. These can provide a robust way towards universal quantum computation, because the geometric phases are determined by the global properties of the evolution paths and possess a built-in noise-resilience feature against certain types of local noises [10–13]. In particular, nonadiabatic holonomic quantum computation (NHQC) [14–20] designed by shortcuts to adiabatic (STA) methods [21–28] makes the computation fast and robust against local parameter fluctuations over the cyclic evolution. However, previous work [2–4, 14–20, 29–39] generally focused on implementing NHQC with physical qubits, which have difficulties in achieving quantum error correction [40–43], due to the huge physical resource overhead and the difficulties in scaling up the number of qubits [43–52].

Therefore, implementing holonomic computation via bosonic codes [53, 54] has attracted much interest recently [55, 56], because a bosonic mode can provide a large Hilbert space, which allows quantum error correction encoding by only extending excitation numbers while keeping the noise channels fixed. Thus, one can realize fault-tolerant quantum computation [55–70] without huge physical resources. For instance, the binomial codes [61] formed from superposition of Fock states are protected to a given order in the time step against continuous dissipative evolution under loss, gain, and dephasing errors. Then, one can correct the quantum errors to an arbitrary order, which can be expanded in

terms of the bosonic creation or destruction operators. However, due to the harmonicity of the bosonic mode, manipulating these photonic states is more difficult than atomic states. This makes it difficult to implement the STA-based NHQC [14, 17, 18] with binomial codes, because the STA-based NHQC usually requires multiple time-dependent control fields to manipulate the system states and the phases; while it is a challenge to realize such control fields based on the previous works [37, 45, 55–71]. Note that the first experiment for binomial-code conditional geometric gates was recently realized [62] using 3D superconducting cavities, but it is not a holonomic computation.

In this manuscript, to overcome the above problems, we propose to use the dressed-state properties of ultrastrong coupling (USC) and deep-strong coupling (DSC) systems [72–78]. Here, the USC-DSC systems describing light-matter coupling beyond the rotating wave approximation (RWA) can give rise to many interesting physical effects [77–90]. In particular, due to the counter-rotating effects, the dressed states of a USC-DSC system are light-matter entangled states. Such dressed states can be used as intermediates [91–95] to couple different Fock basis and induce population transitions between them. This allows to generate and manipulate superposition of Fock states [96–98] by driving the atoms (rather than the cavity), so as to implement the STA-based NHQC with binomial codes.

We design the control fields by the STA method of invariant-based reverse engineering [28, 99–101], thus the generation is fast and robust against pulse imperfections. Moreover, the USC-DSC system allows to apply strong driving fields [93, 94, 102], thus the computing time can

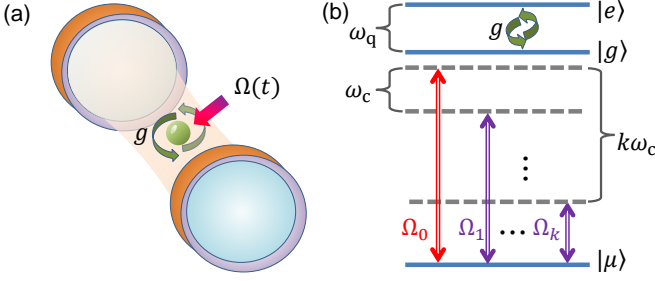


FIG. 1. (a) Schematic illustration of an atom-cavity combined system. (b) Level diagram of the bare three-level atom. The upper two levels ( $|e\rangle, |g\rangle$ ) of the atom are ultrastrongly coupled to the cavity mode with strength  $g$ . The lower two levels ( $|\mu\rangle, |\mu\rangle$ ) are off-resonantly driven by a composite pulse  $\Omega(t) = \sum_k \Omega_k(t) \cos(\omega_k t + \phi_k)$ .

be improved to *nanoseconds*, which can be smaller than the cavity-photon lifetime. This makes our protocols robust against decoherence caused by the relaxations and the dephasings of both the cavity and the atom. Additionally, the present NHQC is scalable for multi-qubit gates. For instance, when ultrastrongly coupling the atom to a bimodal cavity, universal two-qubit geometric gates can be implemented by the same strategy as that for the single-qubit case.

*Model and effective Hamiltonian.*—The basic idea can be realized in a system with an artificial atom ultrastrongly coupled to a cavity mode with coupling strength  $g$  [see Fig. 1(a)]. The atom-cavity interaction can be described by the Rabi Hamiltonian

$$H_R = \omega_c a^\dagger a + \frac{\omega_q}{2} \sigma_g^z + g(a + a^\dagger) \sigma_g^x. \quad (1)$$

Here,  $\sigma_g^x = |e\rangle\langle g| + |g\rangle\langle e|$  and  $\sigma_g^z = |e\rangle\langle e| - |g\rangle\langle g|$  are Pauli matrices,  $a$  ( $a^\dagger$ ) is the annihilation (creation) operator of the cavity field, and  $\omega_{c,(q)}$  is the cavity (qubit) frequency. The dressed states of  $H_R$  can be described by ( $m = 0, 1, 2, \dots$ )

$$|\zeta_m\rangle = \sum_n (c_m^n |g\rangle |n\rangle + d_m^{n\pm1} |e\rangle |n\pm1\rangle), \quad (2)$$

where  $|n\rangle$  denote the Fock states of the cavity. The real coefficients  $c_m^n = \langle \zeta_m | g \rangle |n\rangle$  and  $d_m^{n\pm1} = \langle \zeta_m | e \rangle |n\pm1\rangle$  can be obtained numerically. To generate arbitrary Fock states, we introduce a third ancillary atomic level  $|\mu\rangle$  at a lower energy  $\omega_\mu$  [see Fig. 1(b)]. Then, the eigenstates  $|\mathcal{E}_j\rangle$  with corresponding eigenvalues  $\xi_j$  ( $j = 0, 1, 2, \dots$ ) of the whole system can be separated into (i) noninteracting sectors  $|\mu\rangle |n\rangle$  with eigenvalues  $\omega_\mu + n\omega_c$ ; and (ii) dressed atom-cavity states  $|\zeta_m\rangle$  with eigenvalues  $E_m$ .

Thus, we can couple the states  $|\mu\rangle |n\rangle$  and  $|\zeta_m\rangle$  by driving the atomic transition, e.g.,  $|\mu\rangle \leftrightarrow |g\rangle$ , with a Hamiltonian  $H_D(t) = \Omega(t) \sigma_\mu^x = \Omega(t) (|\mu\rangle\langle g| + |g\rangle\langle \mu|)$ . Here,  $\Omega(t) = \sum_k \Omega_k(t) \cos(\omega_k t + \phi_k)$  is a composite pulse with amplitudes  $\Omega_k(t)$ , frequencies  $\omega_k$ ,

and phases  $\phi_k$ . The total Hamiltonian becomes  $H_{\text{tot}}(t) = \sum_j \xi_j |\mathcal{E}_j\rangle\langle \mathcal{E}_j| + H_D(t)$ . When choosing the frequencies  $\omega_k = (E_m - \omega_\mu - k\omega_c)$  and  $\omega_c \gg \Omega_k(t)$ , the effective Hamiltonian under the RWA is (see details in [103])

$$H_{\text{eff}}(t) = \frac{1}{2} \sum_{k=0}^{k_{\max}} c_m^k \Omega_k(t) e^{i\phi_k} |\mu\rangle |k\rangle \langle \zeta_m| + \text{H.c.}, \quad (3)$$

which describes transitions between the Fock states  $|k\rangle$  through the dressed intermediate state  $|\zeta_m\rangle$ . We can assume  $\omega_\mu = E_m - (k_{\max} + 0.25)\omega_c$ , so that the dressed state  $|\zeta_m\rangle$  is the highest level in the evolution subspace.

*Generation of Fock states and their superpositions.*—Generally, when the initial state is  $|\mu\rangle |0\rangle$ , we can generate even-number Fock states and their superpositions, while when the initial state is  $|\mu\rangle |1\rangle$ , we can generate the odd-number ones. For simplicity, we illustrate the generation of the even-number ones in the following. We assume  $\phi_k = 0$ ,  $c_m^0 \Omega_0(t) = \Omega_p(t)$  and  $c_m^{k'} \Omega_{k'}(t) = \epsilon_{k'} \Omega_s(t)$  ( $k' \neq 0$ ), where  $\epsilon_{k'}$  are time-independent coefficients satisfying  $\sum_{k'} |\epsilon_{k'}|^2 = 1$  and  $\Omega_{p,s}(t)$  is the pump (Stokes) pulse for an effective  $\Lambda$ -type transition. Then,  $H_{\text{eff}}(t)$  becomes

$$H_{\text{eff}}(t) = \frac{1}{2} [\Omega_p(t) |\mu\rangle |0\rangle + \Omega_s(t) |\mu\rangle |\bar{k}'\rangle] \langle \zeta_m| + \text{H.c..} \quad (4)$$

Here,  $|\bar{k}'\rangle = \sum_{k'} \epsilon_{k'} |k'\rangle$  is a superposition of even-number Fock states.

A dynamical invariant of  $H_{\text{eff}}(t)$  satisfying  $\partial_t I(t) = i[H_{\text{eff}}(t), I(t)]$  is [100, 101, 104]

$$I(t) = \cos \varphi (\sin \beta |\mu\rangle |0\rangle + \cos \beta |\mu\rangle |\bar{k}'\rangle) \langle \zeta_m| + i \sin \varphi |\mu\rangle \langle \mu| \otimes |\bar{k}'\rangle \langle 0| + \text{H.c..} \quad (5)$$

Here, we have omitted the explicit time dependence of the parameters  $\beta$  and  $\varphi$ . By imposing  $[I(0), H_{\text{eff}}(0)] \simeq [I(t_f), H_{\text{eff}}(t_f)] \simeq 0$ , the evolution is along  $|\psi_0(t)\rangle = \cos \varphi (\cos \beta |0\rangle - \sin \beta |\bar{k}'\rangle) |\mu\rangle - i \sin \varphi |\zeta_2\rangle$ , which is an eigenstate of the invariant  $I(t)$ . Meanwhile, the driving fields are

$$\begin{aligned} \Omega_p(t) &= \Omega_p(\beta, \varphi) = 2(\dot{\beta} \cot \varphi \sin \beta + \dot{\varphi} \cos \beta), \\ \Omega_s(t) &= \Omega_s(\beta, \varphi) = 2(\dot{\beta} \cot \varphi \cos \beta - \dot{\varphi} \sin \beta). \end{aligned} \quad (6)$$

Such an evolution acquires a dynamical phase and a geometric phase [99]

$$\begin{aligned} \vartheta &= - \int_0^{t_f} \langle \psi_0(t) | H_{\text{eff}}(t) | \psi_0(t) \rangle dt, \\ \Theta &= \int_0^{t_f} \langle \psi_0(t) | i \partial_t | \psi_0(t) \rangle dt, \end{aligned} \quad (7)$$

respectively, which are useful for NHQC discussed later.

To generate arbitrary superposition of Fock states, we choose  $\beta = \beta_0 / [1 + \exp(-t/\tau + T/2\tau)]$  and  $\varphi = \varphi_0 / \exp(t/\tau_c - T/2\tau_c)^2$  [106, 107]. Here,  $\beta_0$  ( $\varphi_0$ ) controls the maximum population of the state  $|\mu\rangle |\bar{k}'\rangle$  ( $|\zeta_m\rangle$ ),

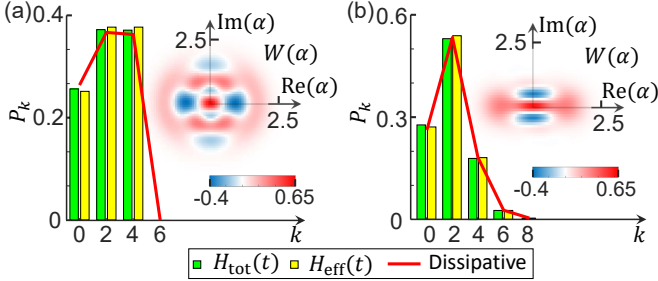


FIG. 2. Histograms of Fock-state populations calculated with the total Hamiltonian  $H_{\text{tot}}(t)$  (green) and the effective Hamiltonian  $H_{\text{eff}}(t)$  (yellow). The red-solid piecewise linear in each panel denotes the Fock-state population calculated by the master equation in Eq. (12), when the dissipation and dephasing rates are  $\gamma_{g,(\mu)} = \gamma_{g,(\mu)}^\phi = 0.5 \times 2\pi$  MHz and  $\kappa = \kappa^\phi = 10^{-2} \times 2\pi$  MHz. Insets show the Wigner function  $W(\alpha)$  of the generated states. (a) The superposition state  $|\tilde{0}\rangle - \sqrt{3/2}(|2\rangle + |4\rangle)/2$  with parameters  $\beta_0 = \pi/3$ ,  $\epsilon_{2,(4)} = 1/\sqrt{2}$ , and  $g = 0.7\omega_c$ . (b) The Cat state  $|\mathcal{C}_e^\eta\rangle$  with amplitude  $\eta = g/\omega_c = \sqrt{2}$ . Other parameters for the driving fields are  $\phi_k = 0$ ,  $\varphi_0 = \pi/5$ ,  $\tau = 0.115T$ , and  $\tau_c = 0.3T$  to satisfy the boundary conditions below Eq. (5). Using the realistic frequencies  $\omega_c = \omega_q = 6.25 \times 2\pi$  GHz for USC [105], the evolution time for each panel is  $T = 35$  ns.

$T$  is the total evolution time,  $\tau$  and  $\tau_c$  determine the boundary conditions. For instance, when choosing  $|\zeta_2\rangle$  as the intermediate state, with parameters  $\beta_0 = \pi/3$  and  $\epsilon_{2,(4)} = 1/\sqrt{2}$ , we can generate the superposition state  $|\tilde{0}\rangle - \sqrt{3/2}(|2\rangle + |4\rangle)/2$  as shown in Fig. 2(a). This figure shows the populations  $P_k = \langle \mu | \langle k | \rho(t_f) | k \rangle | \mu \rangle$  and the Wigner function  $W(\alpha) = 2\text{Tr}[D_\alpha^\dagger \rho(t_f) D_\alpha e^{i\pi a^\dagger a}] / \pi$  at the final time  $t_f$ , where  $\rho(t)$  is the density matrix and  $D_\alpha = \exp(\alpha a^\dagger - \alpha^* a)$  is the displacement operator. We can find that the full dynamics [see the green histograms in Fig. 2(a)] is in excellent agreement with the effective dynamics [the yellow histograms in Fig. 2(a)]. This protocol can also be used to generate Schrödinger's cat states [108–110], e.g., the even cat state  $|\mathcal{C}_e^\eta\rangle = e^{|\eta|^2/2} \sqrt{\text{sech}|\eta|^2} (|\eta\rangle + |-\eta\rangle)/2$  [see Fig. 2(b)], by assuming the intermediate state as  $|\zeta_0\rangle$  and parameters  $\beta_0 = \arccos(\sqrt{\text{sech}|\eta|^2})$ ,  $\epsilon_{k'} = -(\eta^{k'} \cot \beta_0) / \sqrt{k'!}$ , where  $\eta$  is the amplitude of the coherent state  $|\eta\rangle$ .

*NHQC via binomial codes.*—An example of the binomial codes [61] for single-qubit gates protecting against the single-photon loss error is

$$|\tilde{1}\rangle = |2\rangle, \quad |\tilde{0}\rangle = (|0\rangle + |4\rangle)/\sqrt{2}, \quad (8)$$

which form a computational subspace  $\mathcal{S}_c = \{|\tilde{0}\rangle, |\tilde{1}\rangle\}$ . With this definition, a photon loss error brings the logical code words to a subspace with odd photon numbers that is clearly disjoint from the even-parity subspace of the logical code words [61]. The Knill-Laflamme condition [111, 112] for this kind of codes reads  $\langle \tilde{\varrho} | a^\dagger a | \tilde{\varrho} \rangle = 2$

( $\varrho, \varrho' = 0, 1$ ). This means that the probability of a photon jump to occur (or not to occur) is the same for both of the states  $|\tilde{0}\rangle$  and  $|\tilde{1}\rangle$ , implying that the quantum state is not deformed under the error of a photon loss. For instance, when encoding quantum information as  $|\tilde{\psi}_0\rangle = \cos \tilde{\chi} |\tilde{0}\rangle + \sin \tilde{\chi} |\tilde{1}\rangle$ , a photon jump leads to  $|\tilde{\psi}_1\rangle = a |\tilde{\psi}_0\rangle / \sqrt{\langle \tilde{\psi}_0 | a^\dagger a | \tilde{\psi}_0 \rangle} = \cos \tilde{\chi} |3\rangle + \sin \tilde{\chi} |1\rangle$ , which means the information ( $\cos \tilde{\chi}$  and  $\sin \tilde{\chi}$ ) is not deformed [61].

To implement NHQC via the binomial codes, we consider  $|\zeta_2\rangle$  to be the intermediate state. The driving amplitudes are assumed to satisfy  $c_2^0 \Omega_0(t) = c_2^4 \Omega_4(t)$ ,  $\sqrt{2} c_2^0 \Omega_0(t) / c_2^2 \Omega_2(t) = \tan(2\theta)$ , and  $\tilde{\Omega}_0(t) = \sqrt{\sum_k [c_2^k \Omega_k(t)]^2}$ , where  $k \in (0, 2, 4)$  and  $\theta$  is time-independent. Then,  $H_{\text{eff}}(t)$  becomes

$$\tilde{H}_{\text{eff}}(t) = \frac{1}{2} \tilde{\Omega}_0(t) e^{i\phi_2} |\mu\rangle \langle b| \langle \zeta_2| + \text{H.c.}, \quad (9)$$

where  $|b\rangle = e^{-i\phi} \sin(\theta/2) |\tilde{0}\rangle + \cos(\theta/2) |\tilde{1}\rangle$ . The phases of the driving fields are  $\phi_0 = \phi_4$  and  $\phi_2 = \phi_0 - \phi$ .

Initially, quantum information is stored in the logical qubit states of the computational subspace  $\mathcal{S}_c$ . According to [99],  $\tilde{H}_{\text{eff}}(t)$  can drive the system to evolve parallelly along the user-defined paths  $|\tilde{\psi}_+(t)\rangle = \sin(\tilde{\varphi}/2) |\mu\rangle |b\rangle + ie^{-i\tilde{\beta}} \cos(\tilde{\varphi}/2) |\zeta_2\rangle$  and  $|\tilde{\psi}_-(t)\rangle = ie^{i\tilde{\beta}} \cos(\tilde{\varphi}/2) |\mu\rangle |b\rangle + \sin(\tilde{\varphi}/2) |\zeta_2\rangle$ , when  $\tilde{\Omega}_0(t) \sin \phi_2 \equiv \Omega_p(\tilde{\beta}, \tilde{\varphi})/2$  and  $\tilde{\Omega}_0(t) \cos \phi_2 \equiv \Omega_s(\tilde{\beta}, \tilde{\varphi})/2$ . Here,  $\tilde{\beta}$  and  $\tilde{\varphi}$  are time-dependent parameters satisfying  $\tilde{\varphi}(0) = \tilde{\varphi}(t_f)$  for a cyclic evolution. When designing  $\tilde{\varphi} = \pi \sin^2(\pi t/T)$  and

$$\tilde{\beta} = \frac{2}{3} \begin{cases} 2 \sin^3 \tilde{\varphi}, & t \in [0, t_f/2] \\ 2 \sin^3 \tilde{\varphi} - 3\Theta_s, & t \in [t_f/2, t_f] \end{cases} \quad (10)$$

the evolution is along  $|\tilde{\psi}_-(t)\rangle$ , which acquires only a geometric phase of  $2\Theta_s$  [103] according to Eq. (7). Actually, this set of parameters can counteract the systematic errors induced by imperfections of the control fields  $\Omega_k(t)$  [18, 19, 113], making the computation insensitive to such errors (see [103] for more details). In the presence of such imperfections, the driving fields should be corrected as  $\Omega_k^i(t) = (1 + \delta_i) \Omega_k(t)$ , where  $\delta_i$  is an error coefficient.

In the computational subspace  $\mathcal{S}_c$ , the evolution operator is described by

$$U_T = \begin{pmatrix} \cos \Theta_s + i \sin \Theta_s \cos \theta & i \sin \Theta_s \sin \theta e^{i\phi} \\ i \sin \Theta_s \sin \theta e^{-i\phi} & \cos \Theta_s - i \sin \Theta_s \cos \theta \end{pmatrix},$$

which is a universal single-qubit gate. Here, we have omitted a global phase  $\Theta_s$ . We can calculate the average fidelity of a gate over all possible initial states in the subspace  $\mathcal{S}_c$  according to [114, 115]

$$\bar{F} = [\text{Tr}(MM^\dagger) + |\text{Tr}(M)|^2] / (D^2 + D), \quad (11)$$

with  $M = \mathcal{P}_c U_T^\dagger U \mathcal{P}_c$ . Here,  $\mathcal{P}_c$  and  $D$  are the projector and the dimension of the computational subspace  $\mathcal{S}_c$ ,

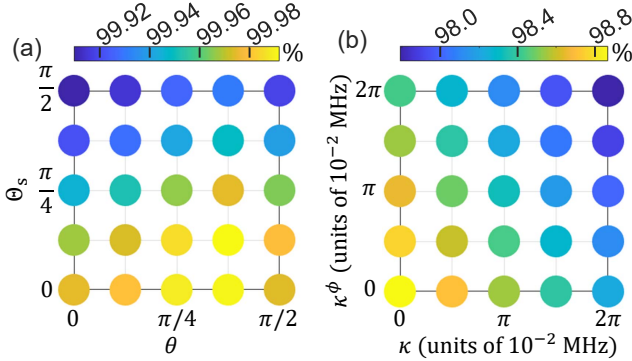


FIG. 3. (a) Average fidelities  $\bar{F}$  of arbitrary single-qubit gates in the presence of pulse imperfections with an error coefficient  $\delta_i = 0.1$ . Each circle denotes a single-qubit gate, e.g.,  $(\Theta_s, \theta) = (\pi/2, \pi/4)$  corresponds to the Hadamard gate. Here, we assume  $\phi = 0$ ,  $T = 150$  ns, and  $g = 0.8\omega_c$ . (b) Fidelity  $F_{\text{out}}$  of the output state  $|\psi_{\text{out}}\rangle = U_T |\psi_{\text{in}}\rangle$  versus the cavity decay  $\kappa$  and dephasing  $\kappa^\phi$ , when  $(\Theta_s, \theta, \phi) = (\pi/2, \pi/4, 0)$  (i.e., the Hadamard gate). The atomic decay and dephasing rates are  $\gamma_{g,(\mu)} = \gamma_{g,(\mu)}^\phi = 0.5 \times 2\pi$  MHz. Other parameters are  $\delta_i = 0.1$ ,  $T = 35$  ns,  $g = 0.8\omega_c$ , and  $\omega_q = \omega_c = 6.25 \times 2\pi$  GHz. With these parameters, the peak amplitudes of the drivings are  $\Omega_k^{\text{peak}} \sim 300 \times 2\pi$  MHz.

respectively. The evolution operator  $U$  is calculated with the total Hamiltonian  $H_{\text{tot}}(t)$ . Figure 3(a) shows the average fidelity  $\bar{F}$  for arbitrary gates in the presence of pulse imperfections. As shown, we can achieve  $\bar{F} \gtrsim 99.9\%$  for arbitrary single-qubit gates with an error coefficient  $\delta_i = 0.1$ , indicating that the generated gates are insensitive to systematic errors.

*Robustness against decoherence.*—In the USC-DSC regime, relaxation and dephasing are usually studied in the basis  $|\mathcal{E}_j\rangle$ , which diagonalizes the whole system. According to Refs. [90–93, 116], the master equation in the Born-Markov approximation valid for generic hybrid-quantum systems is

$$\begin{aligned} \dot{\rho}(t) &= i[\rho(t), H_{\text{tot}}(t)] + \sum_{\nu=0}^3 \mathcal{D} \left[ \sum_j \sqrt{\Lambda_\nu^{jj}} |\mathcal{E}_j\rangle \langle \mathcal{E}_j| \right] \rho(t) \\ &\quad + \sum_{\nu'=0}^5 \sum_{j>j',j'} \Gamma_{\nu'}^{jj'} \mathcal{D}[|\mathcal{E}_{j'}\rangle \langle \mathcal{E}_j|] \rho(t). \end{aligned} \quad (12)$$

Here,  $\mathcal{D}[\mathcal{O}] \rho(t) = \mathcal{O} \rho(t) \mathcal{O}^\dagger - [\rho(t) \mathcal{O}^\dagger \mathcal{O} + \mathcal{O}^\dagger \mathcal{O} \rho(t)]/2$  is the Lindblad superoperator. For simplicity, the dephasing ( $\Lambda_\nu^{jj}$ ) and relaxation ( $\Gamma_{\nu'}^{jj'}$ ) parameters have been written in a compact form [117].

The red-solid piecewise linear in each panel of Fig. 2 denotes the Fock-state populations in the presence of decoherence. When the decay and dephasing rates [117] are  $\gamma_{g,(\mu)} = \gamma_{g,(\mu)}^\phi = 0.5 \times 2\pi$  MHz and  $\kappa = \kappa^\phi = 10^{-2} \times 2\pi$  MHz, the populations calculated by the master equation are almost the same as those by the coherent dynamics, indicating that our protocol for the state

generations is robust against decoherence.

To check the robustness of the geometric gates against decoherence, we assume the input state as  $|\psi_{\text{in}}\rangle = |\tilde{0}\rangle$ , corresponding to an output state  $|\psi_{\text{out}}\rangle = U_T |\psi_{\text{in}}\rangle$ . Using  $(\Theta_s, \theta, \phi) = (\pi/2, \pi/4, 0)$  (Hadamard gate) as an example, in Fig. 3(b), we show the fidelity  $F_{\text{out}} = \langle \psi_{\text{out}} | \rho(t_f) | \psi_{\text{out}} \rangle$  of the output state versus the cavity decay rate  $\kappa$  and dephasing rate  $\kappa^\phi$ , when  $\gamma_{g,(\mu)} = \gamma_{g,(\mu)}^\phi = 0.5 \times 2\pi$  MHz and  $\delta_i = 0.1$ . As shown, when  $\kappa = \kappa^\phi = 0$ , we find  $F_{\text{out}} \gtrsim 99\%$ , indicating that our protocol is mostly insensitive to the atomic decay and dephasing. The influence of the cavity decay and dephasing can only reduce the fidelity of the output state, e.g., from  $F_{\text{out}} \sim 99.0\%$  (when  $\kappa = \kappa^\phi = 0$ ) to  $F_{\text{out}} \sim 98.0\%$  (when  $\kappa = \kappa^\phi = 10^{-2} \times 2\pi$  MHz). Thus, we have demonstrated that our protocol for NHQC is robust against decoherence.

*Multi-qubit gates.*—Our protocol can be extended to implement multi-qubit holonomic gates. For instance, by ultrastrongly coupling the  $\Xi$ -type atom to a bimodal cavity (*a* and *b*) of frequencies  $\omega_a$  and  $\omega_b$ , the atom-cavity interaction can be described by

$$H'_R = \omega_a a^\dagger a + \omega_b b^\dagger b + \frac{\omega_q}{2} \sigma_g^z + \sigma_g^x (g_a a + g_b b + \text{H.c.}),$$

where  $g_a$  and  $g_b$  are coupling strengths. The driving Hamiltonian  $H_D(t)$  can induce transitions between the two-mode Fock states  $|\mathcal{K}\rangle = |k_a\rangle_a |k_b\rangle_b$  through the dressed state  $|\zeta'_m\rangle$  of  $H'_R$  (see details in [103]). By using the same strategy as the single-qubit case, we obtain

$$H'_{\text{eff}}(t) = \frac{1}{2} \sum_{\mathcal{K}=k_a,k_b} c_m^{\mathcal{K}} \Omega_{\mathcal{K}}(t) e^{i\phi_{\mathcal{K}}} |\mu\rangle |\mathcal{K}\rangle \langle \zeta'_m| + \text{H.c.},$$

where  $c_m^{\mathcal{K}} = \langle \zeta'_m | g | \mathcal{K} \rangle$ . Hence, by choosing suitable parameters,  $H'_{\text{eff}}(t)$  becomes similar to  $\tilde{H}_{\text{eff}}(t)$ , thus one can implement universal two-qubit geometric gates via the binomial codes  $\{|\tilde{0}\rangle_a |\tilde{0}\rangle_b, |\tilde{0}\rangle_a |\tilde{1}\rangle_b, |\tilde{1}\rangle_a |\tilde{0}\rangle_b, |\tilde{1}\rangle_a |\tilde{1}\rangle_b\}$ .

*Conclusion.*—We have investigated the possibility of using USC-DSC systems as intermediates for the implementation of *fast, robust, and fault-tolerant* holonomic computations. The dressed-state properties of the USC-DSC systems allow to *simultaneously couple* the dressed state  $|\zeta_m\rangle$  to multiple Fock states, such that one can manipulate the population and the phase of each Fock state as desired. The binomial codes formed from these Fock states can exactly *correct errors* caused by the single-photon loss, making the computation fault-tolerant. Moreover, by designing the pulses with invariant-based engineering, we can eliminate the dynamical phase and achieve only the geometric phase in a cyclic evolution. Such a control technique is compatible with the systematic-error-sensitivity nullification method, making the evolution mostly insensitive to the systematic errors caused by pulse imperfections. Additionally, the USC-DSC regime

allows to apply relatively strong driving fields, such that our protocols are fast. As results, our protocols are robust against the decays and dephasings of the cavity and the atom. Note that this work can generate and manipulate arbitrary superposition of Fock states. The proposed idea can be generalized to realize NHQC with other bosonic qubits, such as cat-qubits [55, 58], for fast, robust, and fault-tolerant quantum computation.

The proposed protocols can be realized in superconducting circuits [74, 75, 105, 118–131]. For instance, by inductively coupling a flux qubit and an *LC* oscillator via Josephson junctions, light-matter coupling strength  $g/\omega_c \sim 1.34$  has been reached in experiments [105]. The quantized level structure in Fig. 1(b) can be realized by adjusting the externally applied magnetic flux [91–93]. Therefore, our proposal works well in the USC-DSC regime, and it may find compelling applications for quantum information processing for various USC-DSC systems, in particular, superconducting systems.

We acknowledge helpful discussions with Y.-H. Kang and Z.-B. Yang. Y.-H.C. is supported by the Japan Society for the Promotion of Science (JSPS) KAKENHI Grant No. JP19F19028. X.W. is supported by the China Postdoctoral Science Foundation No. 2018M631136, and the Natural Science Foundation of China under Grant No. 11804270. F.N. is supported in part by: NTT Research, Army Research Office (ARO) (Grant No. W911NF-18-1-0358), Japan Science and Technology Agency (JST) (via the Q-LEAP program and the CREST Grant No. JPMJCR1676), Japan Society for the Promotion of Science (JSPS) (via the KAKENHI Grant No. JP20H00134 and the JSPS-RFBR Grant No. JPJSBP120194828), the Asian Office of Aerospace Research and Development (AOARD), and the Foundational Questions Institute Fund (FQXi) via Grant No. FQXi-IAF19-06.

- 
- [7] J. Anandan, “Non-adiabatic non-Abelian geometric phase,” *Phys. Lett. A* **133**, 171–175 (1988).
  - [8] F. Wilczek and A. Zee, “Appearance of gauge structure in simple dynamical systems,” *Phys. Rev. Lett.* **52**, 2111–2114 (1984).
  - [9] L.-A. Wu, P. Zanardi, and D. A. Lidar, “Holonomic quantum computation in decoherence-free subspaces,” *Phys. Rev. Lett.* **95**, 130501 (2005).
  - [10] P. Solinas, P. Zanardi, and N. Zanghì, “Robustness of non-Abelian holonomic quantum gates against parametric noise,” *Phys. Rev. A* **70**, 042316 (2004).
  - [11] S.-L. Zhu and P. Zanardi, “Geometric quantum gates that are robust against stochastic control errors,” *Phys. Rev. A* **72**, 020301 (2005).
  - [12] P. Solinas, M. Sassetti, P. Truini, and N. Zanghì, “On the stability of quantum holonomic gates,” *New J. Phys.* **14**, 093006 (2012).
  - [13] M. Johansson, E. Sjöqvist, L. M. Andersson, M. Ericsson, B. Hessmo, K. Singh, and D. M. Tong, “Robustness of nonadiabatic holonomic gates,” *Phys. Rev. A* **86**, 062322 (2012).
  - [14] Q.-X. Lv, Z.-T. Liang, H.-Z. Liu, J.-H. Liang, K.-Y. Liao, and Y.-X. Du, “Noncyclic geometric quantum computation with shortcut to adiabaticity,” *Phys. Rev. A* **101**, 022330 (2020).
  - [15] Y.-X. Du, X.-X. Yue, Z.-T. Liang, J.-Z. Li, H. Yan, and S.-L. Zhu, “Geometric atom interferometry with shortcuts to adiabaticity,” *Phys. Rev. A* **95**, 043608 (2017).
  - [16] Z.-T. Liang, X. Yue, Q. Lv, Y.-X. Du, W. Huang, H. Yan, and S.-L. Zhu, “Proposal for implementing universal superadiabatic geometric quantum gates in nitrogen-vacancy centers,” *Phys. Rev. A* **93**, 040305 (2016).
  - [17] B.-J. Liu, X.-K. Song, Z.-Y. Xue, X. Wang, and M.-H. Yung, “Plug-and-play approach to nonadiabatic geometric quantum gates,” *Phys. Rev. Lett.* **123**, 100501 (2019).
  - [18] Y.-H. Kang, Z.-C. Shi, B.-H Huang, J. Song, and Y. Xia, “Flexible scheme for the implementation of nonadiabatic geometric quantum computation,” *Phys. Rev. A* **101**, 032322 (2020).
  - [19] D. Daems, A. Ruschhaupt, D. Sugny, and S. Guérin, “Robust quantum control by a single-shot shaped pulse,” *Phys. Rev. Lett.* **111**, 050404 (2013).
  - [20] T. Chen, P. Shen, and Z.-Y. Xue, “Robust and fast holonomic quantum gates with encoding on superconducting circuits,” *Phys. Rev. Appl.* **14**, 034038 (2020).
  - [21] D. Guéry-Odelin, A. Ruschhaupt, A. Kiely, E. Torrontegui, S. Martínez-Garaot, and J. G. Muga, “Shortcuts to adiabaticity: Concepts, methods, and applications,” *Rev. Mod. Phys.* **91**, 045001 (2019).
  - [22] E. Torrontegui, S. Ibáñez, S. Martínez-Garaot, M. Modugno, A. del Campo, D. Guéry-Odelin, A. Ruschhaupt, X. Chen, and J. G. Muga, “Shortcuts to adiabaticity,” *Adv. At. Mol. Opt. Phys.* **62**, 117–169 (2013).
  - [23] X. Chen, A. Ruschhaupt, S. Schmidt, A. del Campo, D. Guéry-Odelin, and J. G. Muga, “Fast optimal frictionless atom cooling in harmonic traps: Shortcut to adiabaticity,” *Phys. Rev. Lett.* **104**, 063002 (2010).
  - [24] M. Demirplak and S. A. Rice, “Adiabatic population transfer with control fields,” *J. Phys. Chem. A* **107**, 9937–9945 (2003).

- [25] M. V. Berry, “Transitionless quantum driving,” *J. Phys. A* **42**, 365303 (2009).
- [26] X. Chen, I. Lizuain, A. Ruschhaupt, D. Guéry-Odelin, and J. G. Muga, “Shortcut to adiabatic passage in two- and three-level atoms,” *Phys. Rev. Lett.* **105**, 123003 (2010).
- [27] A. del Campo, “Shortcuts to adiabaticity by counter-diabatic driving,” *Phys. Rev. Lett.* **111**, 100502 (2013).
- [28] A. Baksic, H. Ribeiro, and A. A. Clerk, “Speeding up adiabatic quantum state transfer by using dressed states,” *Phys. Rev. Lett.* **116**, 230503 (2016).
- [29] J. Zhang, L.-C. Kwek, Erik Sjöqvist, D. M. Tong, and P. Zanardi, “Quantum computation in noiseless subsystems with fast non-abelian holonomies,” *Phys. Rev. A* **89**, 042302 (2014).
- [30] B.-J. Liu, Z.-H. Huang, Z.-Y. Xue, and X.-D. Zhang, “Superadiabatic holonomic quantum computation in cavity QED,” *Phys. Rev. A* **95**, 062308 (2017).
- [31] Z.-Y. Xue, F.-L. Gu, Z.-P. Hong, Z.-H. Yang, D.-W. Zhang, Y. Hu, and J. Q. You, “Nonadiabatic holonomic quantum computation with dressed-state qubits,” *Phys. Rev. Appl.* **7**, 054022 (2017).
- [32] A. A. Abdumalikov Jr., J. M. Fink, K. Juliusson, M. Pechal, S. Berger, A. Wallraff, and S. Filipp, “Experimental realization of non-Abelian non-adiabatic geometric gates,” *Nature* **496**, 482–485 (2013).
- [33] G. Feng, G. Xu, and G. Long, “Experimental realization of nonadiabatic holonomic quantum computation,” *Phys. Rev. Lett.* **110**, 190501 (2013).
- [34] Z. Zhu, T. Chen, X. Yang, J. Bian, Z.-Y. Xue, and X. Peng, “Single-loop and composite-loop realization of nonadiabatic holonomic quantum gates in a decoherence-free subspace,” *Phys. Rev. Appl.* **12**, 024024 (2019).
- [35] C. Zu, W.-B. Wang, L. He, W.-G. Zhang, C.-Y. Dai, F. Wang, and L.-M. Duan, “Experimental realization of universal geometric quantum gates with solid-state spins,” *Nature* **514**, 72–75 (2014).
- [36] Y. Sekiguchi, N. Niikura, R. Kuroiwa, H. Kano, and H. Kosaka, “Optical holonomic single quantum gates with a geometric spin under a zero field,” *Nat. Photon.* **11**, 309–314 (2017).
- [37] Y. Xu, W. Cai, Y. Ma, X. Mu, L. Hu, T. Chen, H. Wang, Y. P. Song, Z.-Y. Xue, Z.-Q. Yin, and L. Sun, “Single-loop realization of arbitrary nonadiabatic holonomic single-qubit quantum gates in a superconducting circuit,” *Phys. Rev. Lett.* **121**, 110501 (2018).
- [38] Y. Wang, Y. Su, X. Chen, and C. Wu, “Dephasing-protected scalable holonomic quantum computation on a Rabi lattice,” *Phys. Rev. Appl.* **14**, 044043 (2020).
- [39] Y. Xu, Z. Hua, T. Chen, X. Pan, X. Li, J. Han, W. Cai, Y. Ma, H. Wang, Y. P. Song, Z.-Y. Xue, and L. Sun, “Experimental implementation of universal nonadiabatic geometric quantum gates in a superconducting circuit,” *Phys. Rev. Lett.* **124**, 230503 (2020).
- [40] D. Gottesman, “An introduction to quantum error correction and fault-tolerant quantum computation,” in *Quantum information science and its contributions to mathematics, Proceedings of Symposia in Applied Mathematics*, Vol. 68 (2010) pp. 13–58.
- [41] P. W. Shor, “Scheme for reducing decoherence in quantum computer memory,” *Phys. Rev. A* **52**, R2493–R2496 (1995).
- [42] A. Steane, “Multiple-particle interference and quantum error correction,” *Proc. Roy. Soc. A* **452**, 2551–2577 (1996).
- [43] A. G. Fowler, M. Mariantoni, J. M. Martinis, and A. N. Cleland, “Surface codes: Towards practical large-scale quantum computation,” *Phys. Rev. A* **86**, 032324 (2012).
- [44] O. Oreshkov, T. A. Brun, and D. A. Lidar, “Fault-tolerant holonomic quantum computation,” *Phys. Rev. Lett.* **102**, 070502 (2009).
- [45] T. Chen and Z.-Y. Xue, “Nonadiabatic geometric quantum computation with parametrically tunable coupling,” *Phys. Rev. Appl.* **10**, 054051 (2018).
- [46] C. Wu, Y. Wang, X.-L. Feng, and J.-L. Chen, “Holonomic quantum computation in surface codes,” *Phys. Rev. Appl.* **13**, 014055 (2020).
- [47] J. Zhang, S. J. Devitt, J. Q. You, and F. Nori, “Holonomic surface codes for fault-tolerant quantum computation,” *Phys. Rev. A* **97**, 022335 (2018).
- [48] J. M. Martinis, “Qubit metrology for building a fault-tolerant quantum computer,” *npj Quan. Inf.* **1**, 1 (2015).
- [49] J. Chiaverini, D. Leibfried, T. Schaetz, M. D. Barrett, R. B. Blakestad, J. Britton, W. M. Itano, J. D. Jost, E. Knill, C. Langer, R. Ozeri, and D. J. Wineland, “Realization of quantum error correction,” *Nature* **432**, 602–605 (2004).
- [50] P. Schindler, J. T. Barreiro, T. Monz, V. Nebendahl, D. Nigg, M. Chwalla, M. Hennrich, and R. Blatt, “Experimental repetitive quantum error correction,” *Science* **332**, 1059–1061 (2011).
- [51] J. Kelly, R. Barends, A. G. Fowler, A. Megrant, E. Jeffrey, T. C. White, D. Sank, J. Y. Mutus, B. Campbell, Y. Chen, Z. Chen, B. Chiaro, A. Dunsworth, I.-C. Hoi, C. Neill, P. J. J. O’Malley, C. Quintana, P. Roushan, A. Vainsencher, J. Wenner, A. N. Cleland, and John M. Martinis, “State preservation by repetitive error detection in a superconducting quantum circuit,” *Nature* **519**, 66–69 (2015).
- [52] G. Waldherr, Y. Wang, S. Zaiser, M. Jamali, T. Schulte-Herbrüggen, H. Abe, T. Ohshima, J. Isoya, J. F. Du, P. Neumann, and J. Wrachtrup, “Quantum error correction in a solid-state hybrid spin register,” *Nature* **506**, 204–207 (2014).
- [53] I. L. Chuang, D. W. Leung, and Y. Yamamoto, “Bosonic quantum codes for amplitude damping,” *Phys. Rev. A* **56**, 1114–1125 (1997).
- [54] D. Gottesman, A. Kitaev, and J. Preskill, “Encoding a qubit in an oscillator,” *Phys. Rev. A* **64**, 012310 (2001).
- [55] V. V. Albert, C. Shu, S. Krastanov, C. Shen, R.-B. Liu, Z.-B. Yang, Robert J. Schoelkopf, M. Mirrahimi, M. H. Devoret, and L. Jiang, “Holonomic quantum control with continuous variable systems,” *Phys. Rev. Lett.* **116**, 140502 (2016).
- [56] V. V. Albert, S. O. Mundhada, A. G., S. Touzard, M. H. Devoret, and L. Jiang, “Pair-cat codes: autonomous error-correction with low-order nonlinearity,” *Quan. Sci. Tech.* **4**, 035007 (2019).
- [57] V. V. Albert, K. Noh, K. Duivenvoorden, D. J. Young, R. T. Brierley, P. Reinhold, C. Vuillot, L. Li, C. Shen, S. M. Girvin, B. M. Terhal, and L. Jiang, “Performance and structure of single-mode bosonic codes,” *Phys. Rev. A* **97**, 032346 (2018).
- [58] M. Mirrahimi, Z. Leghtas, V. V. Albert, S. Touzard, R. J. Schoelkopf, L. Jiang, and M. H. Devoret,

- “Dynamically protected cat-qubits: a new paradigm for universal quantum computation,” *New J. Phys.* **16**, 045014 (2014).
- [59] L. Li, C.-L. Zou, V. V. Albert, S. Muralidharan, S. M. Girvin, and L. Jiang, “Cat codes with optimal decoherence suppression for a lossy bosonic channel,” *Phys. Rev. Lett.* **119**, 030502 (2017).
- [60] W. Cai, Y. Ma, W. Wang, C.-L. Zou, and L. Sun, “Bosonic quantum error correction codes in superconducting quantum circuits,” *arXiv:2010.08699* (2020).
- [61] M. H. Michael, M. Silveri, R. T. Brierley, V. V. Albert, J. Salmilehto, L. Jiang, and S. M. Girvin, “New class of quantum error-correcting codes for a bosonic mode,” *Phys. Rev. X* **6**, 031006 (2016).
- [62] Y. Xu, Y. Ma, W. Cai, X. Mu, W. Dai, W. Wang, L. Hu, X. Li, J. Han, H. Wang, Y. P. Song, Z.-B. Yang, S.-B. Zheng, and L. Sun, “Demonstration of controlled-phase gates between two error-correctable photonic qubits,” *Phys. Rev. Lett.* **124**, 120501 (2020).
- [63] R. W. Heeres, P. Reinhold, N. Ofek, L. Frunzio, L. Jiang, M. H. Devoret, and R. J. Schoelkopf, “Implementing a universal gate set on a logical qubit encoded in an oscillator,” *Nat. Commun.* **8**, 94 (2017).
- [64] S. Zhou, M. Zhang, J. Preskill, and L. Jiang, “Achieving the Heisenberg limit in quantum metrology using quantum error correction,” *Nat. Commun.* **9**, 78 (2018).
- [65] C. J. Axline, L. D. Burkhardt, W. Pfaff, M. Zhang, K. Chou, P. Campagne-Ibarcq, P. Reinhold, L. Frunzio, S. M. Girvin, L. Jiang, M. H. Devoret, and R. J. Schoelkopf, “On-demand quantum state transfer and entanglement between remote microwave cavity memories,” *Nat. Phys.* **14**, 705–710 (2018).
- [66] K. S. Chou, J. Z. Blumoff, C. S. Wang, P. C. Reinhold, C. J. Axline, Y. Y. Gao, L. Frunzio, M. H. Devoret, L. Jiang, and R. J. Schoelkopf, “Deterministic teleportation of a quantum gate between two logical qubits,” *Nature* **561**, 368–373 (2018).
- [67] L. Hu, Y. Ma, W. Cai, X. Mu, Y. Xu, W. Wang, Y. Wu, H. Wang, Y. P. Song, C.-L. Zou, S. M. Girvin, L.-M. Duan, and L. Sun, “Quantum error correction and universal gate set operation on a binomial bosonic logical qubit,” *Nat. Phys.* **15**, 503–508 (2019).
- [68] B. Vlastakis, G. Kirchmair, Z. Leghtas, S. E. Nigg, L. Frunzio, S. M. Girvin, M. Mirrahimi, M. H. Devoret, and R. J. Schoelkopf, “Deterministically encoding quantum information using 100-photon Schrödinger cat states,” *Science* **342**, 607–610 (2013).
- [69] Z. Leghtas, S. Touzard, I. M. Pop, A. Kou, B. Vlastakis, A. Petrenko, K. M. Sliwa, A. Narla, S. Shankar, M. J. Hatridge, M. Reagor, L. Frunzio, R. J. Schoelkopf, M. Mirrahimi, and M. H. Devoret, “Confining the state of light to a quantum manifold by engineered two-photon loss,” *Science* **347**, 853–857 (2015).
- [70] S. Rosenblum, Y. Y. Gao, P. Reinhold, C. Wang, C. J. Axline, L. Frunzio, S. M. Girvin, L. Jiang, M. Mirrahimi, M. H. Devoret, *et al.*, “A CNOT gate between multiphoton qubits encoded in two cavities,” *Nat. Commun.* **9**, 652 (2018).
- [71] A. Grimm, N. E. Frattini, S. Puri, S. O. Mundhada, S. Touzard, M. Mirrahimi, S. M. Girvin, S. Shankar, and M. H. Devoret, “Stabilization and operation of a Kerr-cat qubit,” *Nature* **584**, 205–209 (2020).
- [72] E. K. Irish, “Generalized rotating-wave approximation for arbitrarily large coupling,” *Phys. Rev. Lett.* **99**, 173601 (2007).
- [73] D. Braak, “Integrability of the Rabi model,” *Phys. Rev. Lett.* **107**, 100401 (2011).
- [74] A. F. Kockum, A. Miranowicz, S. De Liberato, S. Savasta, and F. Nori, “Ultrastrong coupling between light and matter,” *Nat. Rev. Phys.* **1**, 19–40 (2019).
- [75] P. Forn-Díaz, L. Lamata, E. Rico, J. Kono, and E. Solano, “Ultrastrong coupling regimes of light-matter interaction,” *Rev. Mod. Phys.* **91**, 025005 (2019).
- [76] C. J. Gan and H. Zheng, “Dynamics of a two-level system coupled to a quantum oscillator: Transformed rotating-wave approximation,” *Euro. Phys. J. D* **59**, 473–478 (2010).
- [77] S. De Liberato, C. Ciuti, and I. Carusotto, “Quantum vacuum radiation spectra from a semiconductor microcavity with a time-modulated vacuum Rabi frequency,” *Phys. Rev. Lett.* **98**, 103602 (2007).
- [78] S. Ashhab and F. Nori, “Qubit-oscillator systems in the ultrastrong-coupling regime and their potential for preparing nonclassical states,” *Phys. Rev. A* **81**, 042311 (2010).
- [79] S. De Liberato, “Light-matter decoupling in the deep strong coupling regime: The breakdown of the Purcell effect,” *Phys. Rev. Lett.* **112**, 016401 (2014).
- [80] J. Casanova, G. Romero, I. Lizuain, J. J. García-Ripoll, and E. Solano, “Deep strong coupling regime of the Jaynes-Cummings model,” *Phys. Rev. Lett.* **105**, 263603 (2010).
- [81] L. Garziano, V. Macrì, R. Stassi, O. Di Stefano, F. Nori, and S. Savasta, “One photon can simultaneously excite two or more atoms,” *Phys. Rev. Lett.* **117**, 043601 (2016).
- [82] X. Wang, A. Miranowicz, H.-R. Li, and F. Nori, “Observing pure effects of counter-rotating terms without ultrastrong coupling: A single photon can simultaneously excite two qubits,” *Phys. Rev. A* **96**, 063820 (2017).
- [83] V. Macrì, F. Nori, and A. F. Kockum, “Simple preparation of Bell and Greenberger-Horne-Zeilinger states using ultrastrong-coupling circuit QED,” *Phys. Rev. A* **98**, 062327 (2018).
- [84] O. Di Stefano, A. Settimeni, V. Macrì, L. Garziano, R. Stassi, S. Savasta, and F. Nori, “Resolution of gauge ambiguities in ultrastrong-coupling cavity quantum electrodynamics,” *Nat. Phys.* **15**, 803–808 (2019).
- [85] D. Z. Rossatto, C. J. Villas-Boas, M. Sanz, and E. Solano, “Spectral classification of coupling regimes in the quantum Rabi model,” *Phys. Rev. A* **96**, 013849 (2017).
- [86] X. Cao, J. Q. You, H. Zheng, A. G. Kofman, and F. Nori, “Dynamics and quantum Zeno effect for a qubit in either a low- or high-frequency bath beyond the rotating-wave approximation,” *Phys. Rev. A* **82**, 022119 (2010).
- [87] M. Cirio, S. De Liberato, N. Lambert, and F. Nori, “Ground state electroluminescence,” *Phys. Rev. Lett.* **116**, 113601 (2016).
- [88] M. Cirio, K. Debnath, N. Lambert, and F. Nori, “Amplified optomechanical transduction of virtual radiation pressure,” *Phys. Rev. Lett.* **119**, 053601 (2017).
- [89] M. Cirio, N. Shammah, N. Lambert, S. De Liberato,

- and F. Nori, “Multielectron ground state electroluminescence,” *Phys. Rev. Lett.* **122**, 190403 (2019).
- [90] F. Beaudoin, J. M. Gambetta, and A. Blais, “Dissipation and ultrastrong coupling in circuit QED,” *Phys. Rev. A* **84**, 043832 (2011).
- [91] R. Stassi, A. Ridolfo, O. Di Stefano, M. J. Hartmann, and S. Savasta, “Spontaneous conversion from virtual to real photons in the ultrastrong-coupling regime,” *Phys. Rev. Lett.* **110**, 243601 (2013).
- [92] O. Di Stefano, R. Stassi, L. Garziano, A. F. Kockum, S. Savasta, and F. Nori, “Feynman-diagrams approach to the quantum Rabi model for ultrastrong cavity QED: Stimulated emission and reabsorption of virtual particles dressing a physical excitation,” *New J. Phys.* **19**, 053010 (2017).
- [93] J.-F. Huang and C. K. Law, “Photon emission via vacuum-dressed intermediate states under ultrastrong coupling,” *Phys. Rev. A* **89**, 033827 (2014).
- [94] R. Stassi, M. Cirio, and F. Nori, “Scalable quantum computer with superconducting circuits in the ultrastrong coupling regime,” *npj Quan. Inf.* **6**, 67 (2020).
- [95] Hiroto Mukai, Akiyoshi Tomonaga, and Jaw-Shen Tsai, “Superconducting quantum annealing architecture with LC resonators,” *J. Phys. Soc. Jpn.* **88**, 061011 (2019).
- [96] Y.-X. L., L. F. Wei, and F. Nori, “Generation of nonclassical photon states using a superconducting qubit in a microcavity,” *Europhys. Lett.* **67**, 941–947 (2004).
- [97] M. Hofheinz, H. Wang, M. Ansmann, R. C. Bialczak, E. Lucero, M. Neeley, A. D. O’Connell, D. Sank, J. Wenner, J. M. Martinis, and A. N. Cleland, “Synthesizing arbitrary quantum states in a superconducting resonator,” *Nature* **459**, 546–549 (2009).
- [98] M. Hofheinz, E. M. Weig, M. Ansmann, R. C. Bialczak, E. Lucero, M. Neeley, A. D. O’Connell, H. Wang, J. M. Martinis, and A. N. Cleland, “Generation of fock states in a superconducting quantum circuit,” *Nature* **454**, 310–314 (2008).
- [99] H. R. Lewis and W. B. Riesenfeld, “An exact quantum theory of the time-dependent harmonic oscillator and of a charged particle in a time-dependent electromagnetic field,” *J. Math. Phys.* **10**, 1458–1473 (1969).
- [100] X. Chen and J. G. Muga, “Engineering of fast population transfer in three-level systems,” *Phys. Rev. A* **86**, 033405 (2012).
- [101] Y.-H. Chen, Y. Xia, Q.-Q. Chen, and J. Song, “Efficient shortcuts to adiabatic passage for fast population transfer in multiparticle systems,” *Phys. Rev. A* **89**, 033856 (2014).
- [102] Y. Wang, J. Zhang, C. Wu, J. Q. You, and G. Romero, “Holonomic quantum computation in the ultrastrong-coupling regime of circuit QED,” *Phys. Rev. A* **94**, 012328 (2016).
- [103] See Supplemental Material including Refs. [18, 19, 99, 113] for detailed derivations and discussions of our main results.
- [104] X. Chen, E. Torrontegui, and J. G. Muga, “Lewis-Riesenfeld invariants and transitionless quantum driving,” *Phys. Rev. A* **83**, 062116 (2011).
- [105] F. Yoshihara, T. Fuse, S. Ashhab, K. Kakuyanagi, S. Saito, and K. Semba, “Superconducting qubit–oscillator circuit beyond the ultrastrong-coupling regime,” *Nat. Phys.* **13**, 44–47 (2016).
- [106] G. S. Vasilev, A. Kuhn, and N. V. Vitanov, “Optimum pulse shapes for stimulated Raman adiabatic passage,” *Phys. Rev. A* **80**, 013417 (2009).
- [107] K. Bergmann, H. Theuer, and B. W. Shore, “Coherent population transfer among quantum states of atoms and molecules,” *Rev. Mod. Phys.* **70**, 1003–1025 (1998).
- [108] V. V. Dodonov, I. A. Malkin, and V. I. Man’ko, “Even and odd coherent states and excitations of a singular oscillator,” *Physica* **72**, 597–615 (1974).
- [109] Y.-X. Liu, L. F. Wei, and F. Nori, “Preparation of macroscopic quantum superposition states of a cavity field via coupling to a superconducting charge qubit,” *Phys. Rev. A* **71**, 063820 (2005).
- [110] M. Kira, S. W. Koch, R. P. Smith, A. E. Hunter, and S. T. Cundiff, “Quantum spectroscopy with Schrödinger-cat states,” *Nat. Phys.* **7**, 799–804 (2011).
- [111] C. H. Bennett, D. P. DiVincenzo, J. A. Smolin, and W. K. Wootters, “Mixed-state entanglement and quantum error correction,” *Phys. Rev. A* **54**, 3824–3851 (1996).
- [112] E. Knill and R. Laflamme, “Theory of quantum error-correcting codes,” *Phys. Rev. A* **55**, 900–911 (1997).
- [113] A. Ruschhaupt, X. Chen, D. Alonso, and J. G. Muga, “Optimally robust shortcuts to population inversion in two-level quantum systems,” *New J. Phys.* **14**, 093040 (2012).
- [114] P. Zanardi and D. A. Lidar, “Purity and state fidelity of quantum channels,” *Phys. Rev. A* **70**, 012315 (2004).
- [115] L. H. Pedersen, N. M. Møller, and K. Mølmer, “Fidelity of quantum operations,” *Phys. Lett. A* **367**, 47–51 (2007).
- [116] R. Stassi and F. Nori, “Long-lasting quantum memories: Extending the coherence time of superconducting artificial atoms in the ultrastrong-coupling regime,” *Phys. Rev. A* **97**, 033823 (2018).
- [117] The dephasing and relaxation parameters have been written in a compact form:  $\Lambda_0^{jj} = \kappa^\phi |\langle \mathcal{E}_j | a^\dagger a | \mathcal{E}_j \rangle|^2$ ,  $\Lambda_1^{jj} = \kappa |\langle \mathcal{E}_j | a^\dagger + a | \mathcal{E}_j \rangle|^2$ ,  $\Lambda_{2,(3)}^{jj} = \gamma_{g,(\mu)}^\phi |\langle \mathcal{E}_j | \sigma_{g,(\mu)}^z | \mathcal{E}_j \rangle|^2$ ,  $\Gamma_0^{jj'} = \kappa^\phi |\langle \mathcal{E}_{j'} | a^\dagger a | \mathcal{E}_j \rangle|^2$ ,  $\Gamma_1^{jj'} = \kappa |\langle \mathcal{E}_{j'} | a^\dagger + a | \mathcal{E}_j \rangle|^2$ ,  $\Gamma_{2,(3)}^{jj'} = \gamma_{g,(\mu)} |\langle \mathcal{E}_{j'} | \sigma_{g,(\mu)}^x | \mathcal{E}_j \rangle|^2$ , and  $\Gamma_{4,(5)}^{jj'} = \gamma_{g,(\mu)}^\phi |\langle \mathcal{E}_{j'} | \sigma_{g,(\mu)}^z | \mathcal{E}_j \rangle|^2$ . Here,  $\kappa$  ( $\kappa^\phi$ ) is the cavity decay (dephasing) rate,  $\gamma_{g,(\mu)}$  is the spontaneous emission rate of the transition  $|e\rangle \rightarrow |g\rangle$  ( $|g\rangle \rightarrow |\mu\rangle$ ), and  $\gamma_{g,(\mu)}^\phi$  is the atomic dephasing rate corresponding to  $\sigma_{g,(\mu)}^z$  ( $\sigma_{\mu}^z = |g\rangle\langle g| - |\mu\rangle\langle \mu|$ ).
- [118] P. D. Nation, J. R. Johansson, M. P. Blencowe, and Franco Nori, “Colloquium: Stimulating uncertainty: Amplifying the quantum vacuum with superconducting circuits,” *Rev. Mod. Phys.* **84**, 1–24 (2012).
- [119] Z. L. Xiang, S. Ashhab, J. Q. You, and F. Nori, “Hybrid quantum circuits: Superconducting circuits interacting with other quantum systems,” *Rev. Mod. Phys.* **85**, 623–653 (2013).
- [120] J. Q. You and F. Nori, “Atomic physics and quantum optics using superconducting circuits,” *Nature* **474**, 589–597 (2011).
- [121] M. H. Devoret, S. Girvin, and R. Schoelkopf, “Circuit-QED: How strong can the coupling between a Josephson junction atom and a transmission line resonator be?” *Ann. Phys.* **16**, 767–779 (2007).
- [122] J. R. Johansson, G. Johansson, and F. Nori, “Optomechanical-like coupling between superconduct-

- ing resonators,” *Phys. Rev. A* **90**, 053833 (2014).
- [123] J. R. Johansson, G. Johansson, C. M. Wilson, and F. Nori, “Dynamical Casimir effect in a superconducting coplanar waveguide,” *Phys. Rev. Lett.* **103**, 147003 (2009).
- [124] T. Niemczyk, F. Deppe, H. Huebl, E. P. Menzel, F. Hocke, M. J. Schwarz, J. J. Garcia-Ripoll, D. Zueco, T. Hümmer, E. Solano, A. Marx, and R. Gross, “Circuit quantum electrodynamics in the ultrastrong-coupling regime,” *Nat. Phys.* **6**, 772–776 (2010).
- [125] P. Forn-Díaz, J. Lisenfeld, D. Marcos, J. J. García-Ripoll, E. Solano, C. J. P. M. Harmans, and J. E. Mooij, “Observation of the Bloch-Siegert shift in a qubit-oscillator system in the ultrastrong coupling regime,” *Phys. Rev. Lett.* **105**, 237001 (2010).
- [126] S. J. Bosman, M. F. Gely, V. Singh, A. Bruno, D. Bothner, and G. A. Steele, “Multi-mode ultrastrong coupling in circuit quantum electrodynamics,” *npj Quantum Inf.* **3**, 46 (2017).
- [127] P. Forn-Díaz, G. Romero, C. J. P. M. Harmans, E. Solano, and J. E. Mooij, “Broken selection rule in the quantum Rabi model,” *Sci. Rep.* **6**, 26720 (2016).
- [128] A. Baust, E. Hoffmann, M. Haeberlein, M. J. Schwarz, P. Eder, J. Goetz, F. Wulschner, E. Xie, L. Zhong, F. Quijandría, D. Zueco, J.-J. García Ripoll, L. García-Álvarez, G. Romero, E. Solano, K. G. Fedorov, E. P. Menzel, F. Deppe, A. Marx, and R. Gross, “Ultrastrong coupling in two-resonator circuit QED,” *Phys. Rev. B* **93**, 214501 (2016).
- [129] Z. Chen, Y. Wang, T. Li, L. Tian, Y. Qiu, K. Inomata, F. Yoshihara, S. Han, F. Nori, J. S. Tsai, and J. Q. You, “Single-photon-driven high-order sideband transitions in an ultrastrongly coupled circuit-quantum-electrodynamics system,” *Phys. Rev. A* **96**, 012325 (2017).
- [130] F. Yoshihara, T. Fuse, S. Ashhab, K. Kakuyanagi, S. Saito, and K. Semba, “Characteristic spectra of circuit quantum electrodynamics systems from the ultrastrong- to the deep-strong-coupling regime,” *Phys. Rev. A* **95**, 053824 (2017).
- [131] F. Yoshihara, T. Fuse, Z. Ao, S. Ashhab, K. Kakuyanagi, S. Saito, T. Aoki, K. Koshino, and K. Semba, “Inversion of qubit energy levels in qubit-oscillator circuits in the deep-strong-coupling regime,” *Phys. Rev. Lett.* **120**, 183601 (2018).

## Supplemental Material

In this Supplemental Material, we first deduce the effective Hamiltonian used in the main text. Then, we show how to use the control method of invariant-based engineering to eliminate dynamical phases and achieve only geometric phases in a non-adiabatic circle evolution. We also show how this control method can minimize the systematic error sensitivity, making the holonomic computation mostly insensitive to the systematic errors. Third, we present a possible implementation of two-qubit holonomic gates via binomial codes.

### S1. Effective Hamiltonian

The total Hamiltonian for this protocol can be written as

$$\begin{aligned} H_{\text{tot}} &= H_0 + H_D(t), \\ H_0 &= \sum_{m=0}^{\infty} E_m |\zeta_m\rangle\langle\zeta_m| + \sum_{n=0}^{\infty} (\omega_\mu + n\omega_c) |\mu\rangle\langle\mu| \otimes |n\rangle\langle n|, \\ H_D(t) &= \Omega(t) (|\mu\rangle\langle g| + |g\rangle\langle\mu|). \end{aligned} \quad (\text{S1})$$

Here,  $|\zeta_m\rangle$  are the dressed eigenstates of the Rabi Hamiltonian with eigenvalues  $E_m$ ,  $\omega_\mu$  denotes the energy of the lowest atomic level  $|\mu\rangle$ ,  $n$  is the cavity photon number, and

$$\Omega(t) = \Omega_k(t) \cos(\omega_k t + \phi_k), \quad (\text{S2})$$

is a composite pulse driving the atomic transition  $|\mu\rangle \leftrightarrow |g\rangle$ . Performing the unitary transformation  $U_d = \exp(-iH_0t)$  and choosing the frequencies as

$$\omega_k = E_m - \omega_\mu - k\omega_c, \quad (\text{S3})$$

we have

$$\begin{aligned} H'_D(t) &= \frac{1}{2} \sum_k \sum_{m'} \sum_n c_{m'}^n \Omega_k(t) |\mu\rangle |n\rangle \langle\zeta_{m'}| \exp[-i\Delta E_{m'} t + i(n-k)\omega_c t + i\phi] \\ &\quad + \exp[-i\Delta E_{m'} t + i(n-k)\omega_c t - 2i\omega_k t - i\phi] + \text{H.c.}, \end{aligned} \quad (\text{S4})$$

where  $\Delta E_{m'} = E_{m'} - E_m$  is the energy gap between the eigenstates  $|\zeta_{m'}\rangle$  and  $|\zeta_m\rangle$ .

Obviously, when satisfying

$$\begin{aligned} c_{m'}^n \Omega_k(t) &\ll |(n-k)\omega_c - \Delta E_{m'}|, \\ c_{m'}^n \Omega_k(t) &\ll |(n-k)\omega_c - 2\omega_k - \Delta E_{m'}|, \end{aligned} \quad (\text{S5})$$

the fast-oscillating terms can be neglected in the rotating wave approximation (RWA). Then, the effective Hamiltonian becomes

$$H_{\text{eff}}(t) = \frac{1}{2} \sum_k c_m^k \Omega_k(t) e^{i\phi_k} |\mu\rangle |k\rangle \langle\zeta_m| + \text{H.c.}, \quad (\text{S6})$$

i.e., the effective Hamiltonian in Eq. (3) of the main text.

### S2. Dynamical invariants

An operator  $I(t)$  satisfying  $\partial_t I(t) = i[H(t), I(t)]$  is a dynamical invariant of an arbitrary Hamiltonian  $H(t)$ . According to [99], an arbitrary solution of the Schrödinger equation

$$i \frac{\partial}{\partial t} |\psi(t)\rangle = H(t) |\psi(t)\rangle, \quad (\text{S7})$$

can be expressed by using the eigenstates of  $I(t)$  as

$$\begin{aligned} |\psi(t)\rangle &= \sum_n C_n e^{i\mathcal{R}_n(t)} |\psi_n(t)\rangle, \\ \mathcal{R}_n(t) &= \int_0^t \langle\psi_n(t')| [i\partial_{t'} - H(t')] |\psi_n(t')\rangle dt', \end{aligned} \quad (\text{S8})$$

where  $C_n$  are time-independent amplitudes,  $|\psi_n(t)\rangle$  are the orthonormal eigenvectors of  $I(t)$ , and  $\mathcal{R}_n(t)$  are the Lewis-Riesenfeld phases [99]. These phases include dynamical phases

$$\vartheta_n(t) = - \int_0^t \langle\psi_n(t')| H(t') |\psi(t')\rangle dt', \quad (\text{S9})$$

and geometric phases

$$\Theta_n(t) = \int_0^t \langle\psi_n(t')| i\partial_{t'} |\psi_n(t')\rangle dt'. \quad (\text{S10})$$

### S3. Dynamical and geometric phases of the holonomic gates

The effective Hamiltonian

$$\tilde{H}_{\text{eff}}(t) = \frac{1}{2} \tilde{\Omega}_0(t) e^{i\phi_2} |\zeta_2\rangle\langle b| \langle\mu| + \text{H.c.}, \quad (\text{S11})$$

in Eq. (9) of the main text for the STA-based NHQC can be regarded as the intermediate state  $|\zeta_2\rangle$  coupled to the bright state

$$|b\rangle = e^{-i\phi} \sin(\theta/2) |\tilde{0}\rangle + \cos(\theta/2) |\tilde{1}\rangle, \quad (\text{S12})$$

but decoupled from the dark state

$$|d\rangle = e^{-i\phi} \cos(\theta/2) |\tilde{1}\rangle - \sin(\theta/2) |\tilde{0}\rangle. \quad (\text{S13})$$

A dynamical invariant of  $\tilde{H}_{\text{eff}}(t)$  is

$$\tilde{I}(t) = \cos \tilde{\varphi} (|\zeta_2\rangle\langle\zeta_2| - |b\rangle\langle b| \otimes |\mu\rangle\langle\mu|) + \left( e^{i\tilde{\beta}} \sin \tilde{\varphi} |\zeta_2\rangle\langle b| \langle\mu| + \text{H.c.} \right), \quad (\text{S14})$$

with eigenvectors

$$\begin{aligned} |\tilde{\psi}_+(t)\rangle &= \sin(\tilde{\varphi}/2) |\mu\rangle |b\rangle + ie^{-i\tilde{\beta}} \cos(\tilde{\varphi}/2) |\zeta_2\rangle, \\ |\tilde{\psi}_-(t)\rangle &= ie^{i\tilde{\beta}} \cos(\tilde{\varphi}/2) |\mu\rangle |b\rangle + \sin(\tilde{\varphi}/2) |\zeta_2\rangle. \end{aligned} \quad (\text{S15})$$

Then, substituting Eqs. (S11) and (S15), into Eq. (S8), the time derivatives of the dynamic phases and geometric phases acquired by  $|\tilde{\psi}_\pm(t)\rangle$  are

$$\dot{\vartheta}_\pm(t) = \mp \frac{\dot{\tilde{\beta}}}{2} \sin \tilde{\varphi} \tan \tilde{\varphi}, \quad \dot{\Theta}_\pm(t) = \pm \frac{\dot{\tilde{\beta}}}{2} (1 - \cos \tilde{\varphi}), \quad (\text{S16})$$

respectively. Obviously,  $\dot{\vartheta}_\pm(t)$  and  $\dot{\Theta}_\pm(t)$  obey the same mathematical symmetry. To eliminate the dynamical phases and achieve only the geometric phases, we can design a piecewise function for  $\tilde{\beta}$ , e.g.,

$$\tilde{\beta} = \begin{cases} f(t), & t \in [0, t_f/2] \\ f(t) - 2\Theta_s, & t \in [t_f/2, t_f] \end{cases} \quad (\text{S17})$$

where  $\Theta_s$  is a constant. Then, we assume  $\dot{\vartheta}_\pm(t - t_f/2)$  to be odd functions, leading to

$$\vartheta_\pm = \mp \int_{\frac{t_f}{2}}^{\frac{t_f}{2} + \Delta t} \Theta_s (\sin \tilde{\varphi} \tan \tilde{\varphi}) dt + \int_0^{t_f} \dot{\vartheta}_\pm(t) dt = \mp \Theta_s \sin \tilde{\varphi} \left( \frac{t_f}{2} \right) \tan \tilde{\varphi} \left( \frac{t_f}{2} \right). \quad (\text{S18})$$

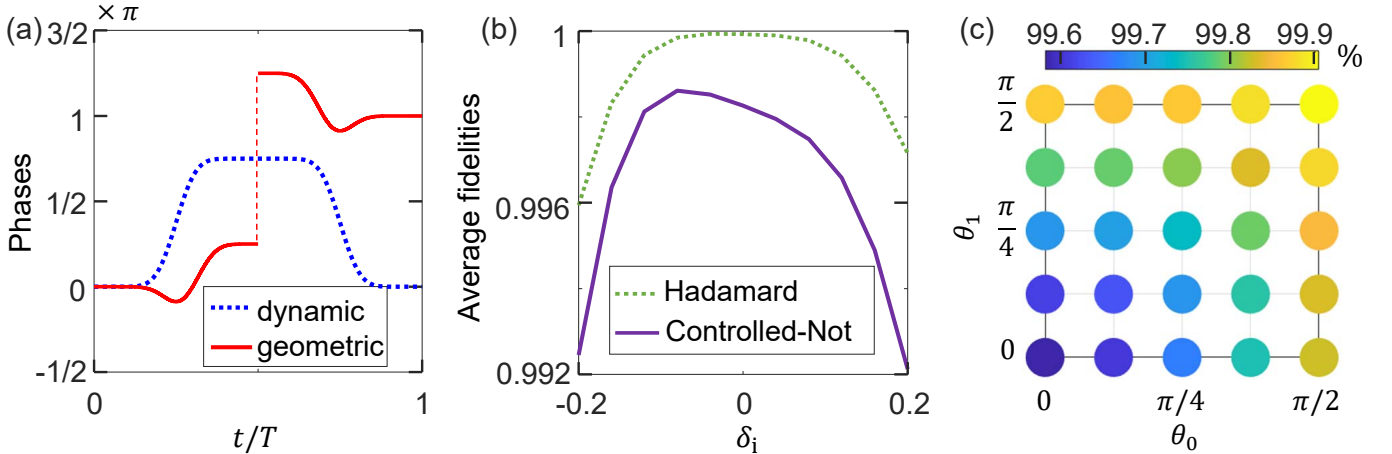


FIG. S1. (a) Dynamical and geometric phases acquired by the evolution along  $|\tilde{\psi}_-(t)\rangle$  with parameters given in Eq. (S21) and  $\Theta_s = \pi/2$ . (b) Average fidelities  $\bar{F}$  of the Hadamard and controlled-Not gates versus the error coefficient  $\delta_i$ . For the Hadamard gate, the intermediate state is  $|\zeta_2\rangle$ ; Parameters are  $T = 150$  ns,  $g = 0.8\omega_c$ ,  $\omega_q = \omega_c = 6.25 \times 2\pi$  GHz, and  $(\Theta_s, \theta, \phi) = (\pi/2, \pi/4, 0)$ . For the controlled-Not gate, the intermediate state is  $|\zeta'_0\rangle$ ; Parameters are  $T = 750$  ns,  $g_a = g_b = 1.3\omega_c$ ,  $\omega_b = 0.9\omega_a$ ,  $\omega_a = \omega_q = 6.25 \times 2\pi$  GHz, and  $(\Theta_s, \theta_0, \theta_1, \theta_2, \phi) = (\pi/2, 0, \pi/2, \pi/2, \pi)$ . (c) Average fidelities of arbitrary two-qubit gates in the presence of pulse imperfections with an error coefficient  $\delta_i = 0.1$ . We assume  $\Theta_s = \pi/2$  and  $\phi = \pi$  for simplicity. Each circle denotes a two-qubit gate, e.g.,  $(\theta_0, \theta_1) = (0, \pi/2)$  corresponds to the controlled-Not gate. Other parameters are the same as those chosen for the controlled-Not gate in the middle panel.

Here,  $\Delta t$  is a small increase in time, and we have assumed  $\tilde{\varphi}$  to be continuous in time. Meanwhile, for the geometric phases,  $\dot{\Theta}_{\pm}(t - t_f/2)$  are also odd functions, leading to

$$\Theta_{\pm} = \mp \int_{\frac{t_f}{2}}^{\frac{t_f}{2} + \Delta t} \Theta_s (1 - \cos \tilde{\varphi}) dt + \int_0^{t_f} \dot{\Theta}_{\pm}(t) dt = \mp \Theta_s \left[ 1 - \cos \tilde{\varphi} \left( \frac{t_f}{2} \right) \right]. \quad (\text{S19})$$

Hence, when  $\tilde{\varphi}(t_f/2) = \pi$ , we have  $\vartheta_{\pm} = 0$  and  $\Theta_{\pm} = \mp 2\Theta_s$ . The evolution only acquires geometric phases [see Fig. S1(a)].

#### S4. Robust control

The systematic errors of laser pulses due to imperfections of devices may be troublesome factors to obtain high fidelities for the gates. In the presence of such imperfections with error parameter  $\delta_i$ , the driving amplitudes become  $\Omega_k^i(t) = (1 + \delta_i)\Omega_k(t)$ . Accordingly, the effective Hamiltonian  $\tilde{H}_{\text{eff}}(t)$  should be corrected as  $\tilde{H}_{\text{eff}}^i(t) = (1 + \delta_i)\tilde{H}_{\text{eff}}(t)$ . By using time-dependent perturbation theory up to  $\mathcal{O}(\delta_i)$ , the evolution state of the system is approximatively

$$|\tilde{\psi}_-^i(t)\rangle \approx |\tilde{\psi}_-(t)\rangle - i\delta_i \int_0^{t_f} U(t_f, t) \tilde{H}_{\text{eff}}^i(t) |\tilde{\psi}_-(t)\rangle dt$$

where  $U(t_f, t)$  is the unperturbed time evolution operator. Here, for simplicity, we have assumed that the evolution is along  $|\tilde{\psi}_-(t)\rangle$  by designing  $\tilde{\varphi}(0) = \tilde{\varphi}(t_f) = 0$ . We assume that the protocol works perfectly when  $\delta_i = 0$ , resulting in

$$P_{\text{out}} \approx 1 - \delta_i^2 \left| \int_0^{t_f} e^{2i\mathcal{R}_-(t)} \langle \tilde{\psi}_+(t) | \tilde{H}_{\text{eff}}(t) | \tilde{\psi}_-(t) \rangle dt \right|^2,$$

where  $P_{\text{out}}$  is the population of the output state after the gate operation. Then, the systematic error sensitivity can be defined as [113]

$$q_i := -\frac{1}{2} \frac{\partial^2 P_{\text{out}}}{\partial \delta_i^2} \Big|_{\delta_i=0} = \left| \int_0^{t_f} e^{i\tilde{\beta} + 2i\mathcal{R}_-(t)} \dot{\tilde{\varphi}} \sin^2 \tilde{\varphi} dt \right|^2. \quad (\text{S20})$$

To minimize  $q_i$ , as discussed in Refs. [18, 19, 113], we can assume

$$\tilde{\varphi} = \pi \sin^2(\pi t/T), \quad f(t) = \frac{4}{3} \sin^3 \tilde{\varphi}, \quad (\text{S21})$$

resulting in  $q_i \simeq 0$ , which means that the holonomic gates are insensitive to the systematic errors induced by the pulse imperfections. For instance, by the green-dash curve in Fig. S1(b), we show the average fidelity  $\bar{F}$  of the Hadamard gate versus the error coefficient  $\delta_i$ . As shown, when  $\delta_i \in [-0.1, 0.1]$ , the average fidelity is nearly 99.9%, indicating that our protocol is insensitive to the systematic error caused by pulse imperfections.

## S5. Two-qubit gates

We consider that the  $\Xi$ -type atom ultrastrongly couples to a bimodal cavity (frequencies  $\omega_a$  and  $\omega_b$ ). The system Hamiltonian is described by

$$\begin{aligned} H'_{\text{tot}} &= H'_{\text{R}} + \omega_\mu |\mu\rangle\langle\mu| + H_{\text{D}}(t), \\ H'_{\text{R}} &= \omega_a a^\dagger a + \omega_b b^\dagger b + \frac{\omega_q}{2} \sigma_g^z + [g_a(a + a^\dagger) + g_b(b + b^\dagger)] \sigma_g^x. \end{aligned} \quad (\text{S22})$$

The eigenstates of  $H'_{\text{R}}$  corresponding to the eigenvalues  $E'_m$  can be described by

$$|\zeta'_m\rangle = \sum_{n_a, n_b, m=0}^{\infty} c_m^{n_a, n_b} |g\rangle |n_a\rangle_a |n_b\rangle_b + d_m^{n_a, n_b} |e\rangle |n_a\rangle_a |n_b\rangle_b,$$

where  $|n_a\rangle_b$  and  $|n_b\rangle_b$  denote the Fock states of the two cavity modes, respectively. Then, we assume that the driving field is

$$\Omega(t) = \Omega_{k_a}^{k_b}(t) \cos(\omega_{k_a}^{k_b} + \phi_{k_a}^{k_b}). \quad (\text{S23})$$

Similar to the derivation from Eq. (S1) to Eq. (S6), when choosing the frequencies that  $\omega_a/\omega_b \neq 0, 1, 2, \dots$ , and

$$\omega_{k_a}^{k_b} = E'_m - \omega_\mu - k_a \omega_a - k_b \omega_b, \quad (\text{S24})$$

the effective Hamiltonian is approximatively

$$H'_{\text{eff}}(t) = \frac{1}{2} \sum_{k_a, k_b} c_m^{k_a, k_b} \Omega_{k_a}^{k_b}(t) \exp(i\phi_{k_a}^{k_b}) |\mu\rangle |k_a\rangle_a |k_b\rangle_b \langle \zeta'_m | + \text{H.c..} \quad (\text{S25})$$

For simplicity, we assume that the intermediate state is the dressed state  $|\zeta'_0\rangle$ , the driving amplitudes are

$$\begin{aligned} c_0^{0,0} \Omega_0^0(t) &= c_0^{0,4} \Omega_0^4(t) = c_0^{4,0} \Omega_4^0(t) = c_0^{4,4} \Omega_4^4(t) = \Xi_{\tilde{0}\tilde{0}}(t)/2, \\ c_0^{0,2} \Omega_0^2(t) &= c_0^{4,2} \Omega_4^2(t) = \Xi_{\tilde{0}\tilde{1}}(t)/\sqrt{2}, \\ c_0^{2,0} \Omega_2^0(t) &= c_0^{2,4} \Omega_2^4(t) = \Xi_{\tilde{1}\tilde{0}}(t)/\sqrt{2}, \\ c_0^{2,2} \Omega_2^2(t) &= \Xi_{\tilde{1}\tilde{1}}(t), \end{aligned} \quad (\text{S26})$$

and the phases are

$$\begin{aligned} \phi_0^0 &= \phi_0^4 = \phi_4^0 = \phi_4^4 = \phi_{\tilde{0}\tilde{0}}, \\ \phi_0^2 &= \phi_4^2 = \phi_{\tilde{0}\tilde{0}} + \phi, \\ \phi_2^0 &= \phi_2^4 = \phi_{\tilde{0}\tilde{0}} + \phi, \\ \phi_2^2 &= \phi_{\tilde{0}\tilde{0}} + \phi. \end{aligned} \quad (\text{S27})$$

Here,  $\phi_{\tilde{0}\tilde{0}}$  is time-dependent and  $\phi$  is time-independent.

The effective Hamiltonian in Eq. (S25) becomes

$$\begin{aligned} \tilde{H}'_{\text{eff}}(t) &= \frac{e^{i\phi_{\tilde{0}\tilde{0}}}}{2} |\mu\rangle [\Xi_{\tilde{0}\tilde{0}}(t) |\tilde{0}\rangle_a |\tilde{0}\rangle_b + \Xi_{\tilde{0}\tilde{1}}(t) e^{i\phi} |\tilde{0}\rangle_a |\tilde{1}\rangle_b + \Xi_{\tilde{1}\tilde{0}}(t) e^{i\phi} |\tilde{1}\rangle_a |\tilde{0}\rangle_b + \Xi_{\tilde{1}\tilde{1}}(t) e^{i\phi} |\tilde{1}\rangle_a |\tilde{1}\rangle_b] \langle \zeta'_0 | + \text{H.c.}, \\ &= \frac{\tilde{\Xi}_0(t) e^{i\phi_{\tilde{0}\tilde{0}}}}{2} |\mu\rangle |b'\rangle \langle \zeta'_0 | + \text{H.c.}, \end{aligned} \quad (\text{S28})$$

with the binomial codes

$$\begin{aligned} |\tilde{0}\rangle_a &= \frac{1}{\sqrt{2}}(|0\rangle_a + |4\rangle_a), \quad |\tilde{1}\rangle_a = |2\rangle_a, \\ |\tilde{0}\rangle_b &= \frac{1}{\sqrt{2}}(|0\rangle_b + |4\rangle_b), \quad |\tilde{1}\rangle_b = |2\rangle_b. \end{aligned} \quad (\text{S29})$$

Here, the bright state  $|b'\rangle$  can be defined as

$$\begin{aligned} |b'\rangle &= [\cos \frac{\theta_0}{2} \cos \frac{\theta_1}{2} |\tilde{0}\rangle_a |\tilde{0}\rangle_b + \exp(i\phi) \cos \frac{\theta_0}{2} \sin \frac{\theta_1}{2} |\tilde{0}\rangle_a |\tilde{1}\rangle_b \\ &\quad + \exp(i\phi) \sin \frac{\theta_0}{2} \cos \frac{\theta_2}{2} |\tilde{1}\rangle_a |\tilde{0}\rangle_b + \exp(i\phi) \sin \frac{\theta_0}{2} \sin \frac{\theta_2}{2} |\tilde{1}\rangle_a |\tilde{1}\rangle_b], \end{aligned} \quad (\text{S30})$$

with auxiliary parameters

$$\begin{aligned} \tilde{\Xi}_0(t) &= \sqrt{[\Xi_{\tilde{0}\tilde{0}}(t)]^2 + [\Xi_{\tilde{0}\tilde{1}}(t)]^2 + [\Xi_{\tilde{1}\tilde{0}}(t)]^2 + [\Xi_{\tilde{1}\tilde{1}}(t)]^2}, \\ \theta_0 &= 2 \arctan \left[ \frac{\sqrt{\Xi_{\tilde{1}\tilde{0}}^2(t) + \Xi_{\tilde{1}\tilde{1}}^2(t)}}{\sqrt{\Xi_{\tilde{0}\tilde{0}}^2(t) + \Xi_{\tilde{0}\tilde{1}}^2(t)}} \right], \\ \theta_1 &= 2 \arctan \left[ \frac{\Xi_{\tilde{0}\tilde{1}}(t)}{\Xi_{\tilde{0}\tilde{0}}(t)} \right], \quad \theta_2 = 2 \arctan \left[ \frac{\Xi_{\tilde{1}\tilde{1}}(t)}{\Xi_{\tilde{1}\tilde{0}}(t)} \right]. \end{aligned} \quad (\text{S31})$$

For simplicity, we choose  $\theta_{0,(1,2)}$  to be time-independent. The orthogonal partners of the state  $|b'\rangle$  are

$$\begin{aligned} |d_1\rangle &= [\sin \frac{\theta_0}{2} \cos \frac{\theta_1}{2} |\tilde{0}\rangle_a |\tilde{0}\rangle_b + \exp(i\phi) \sin \frac{\theta_0}{2} \sin \frac{\theta_1}{2} |\tilde{0}\rangle_a |\tilde{1}\rangle_b \\ &\quad - \exp(i\phi) \cos \frac{\theta_0}{2} \cos \frac{\theta_2}{2} |\tilde{1}\rangle_a |\tilde{0}\rangle_b - \exp(i\phi) \cos \frac{\theta_0}{2} \sin \frac{\theta_2}{2} |\tilde{1}\rangle_a |\tilde{1}\rangle_b], \\ |d_2\rangle &= [\cos \frac{\theta_0}{2} \sin \frac{\theta_1}{2} |\tilde{0}\rangle_a |\tilde{0}\rangle_b - \exp(i\phi) \cos \frac{\theta_0}{2} \cos \frac{\theta_1}{2} |\tilde{0}\rangle_a |\tilde{1}\rangle_b \\ &\quad + \exp(i\phi) \sin \frac{\theta_0}{2} \sin \frac{\theta_2}{2} |\tilde{1}\rangle_a |\tilde{0}\rangle_b - \exp(i\phi) \sin \frac{\theta_0}{2} \cos \frac{\theta_2}{2} |\tilde{1}\rangle_a |\tilde{1}\rangle_b], \\ |d_3\rangle &= [\sin \frac{\theta_0}{2} \sin \frac{\theta_1}{2} |\tilde{0}\rangle_a |\tilde{0}\rangle_b - \exp(i\phi) \sin \frac{\theta_0}{2} \cos \frac{\theta_1}{2} |\tilde{0}\rangle_a |\tilde{1}\rangle_b \\ &\quad - \exp(i\phi) \cos \frac{\theta_0}{2} \sin \frac{\theta_2}{2} |\tilde{1}\rangle_a |\tilde{0}\rangle_b + \exp(i\phi) \cos \frac{\theta_0}{2} \cos \frac{\theta_2}{2} |\tilde{1}\rangle_a |\tilde{1}\rangle_b]. \end{aligned} \quad (\text{S32})$$

Then, by using the same strategy as that of the single-qubit holonomic gates, we design

$$\begin{aligned} \tilde{\Xi}_0(t) \sin \phi_{\tilde{0}\tilde{0}} &= \Omega_p(\tilde{\beta}, \tilde{\varphi})/2 = \dot{\tilde{\beta}} \cot \tilde{\varphi} \sin \tilde{\beta} + \dot{\tilde{\varphi}} \cos \tilde{\beta}, \\ \tilde{\Xi}_0(t) \cos \phi_{\tilde{0}\tilde{0}} &= \Omega_s(\tilde{\beta}, \tilde{\varphi})/2 = \dot{\tilde{\beta}} \cot \tilde{\varphi} \cos \tilde{\beta} - \dot{\tilde{\varphi}} \sin \tilde{\beta}. \end{aligned} \quad (\text{S33})$$

The evolution operator after a cyclic evolution along

$$|\psi'(t)\rangle = ie^{i\tilde{\beta}}(\tilde{\varphi}/2)|\mu\rangle|b\rangle + \sin(\tilde{\varphi}/2)|\zeta'_0\rangle, \quad (\text{S34})$$

in the subspace spanned by  $\{|b'\rangle, |d_1\rangle, |d_2\rangle, |d_3\rangle\}$  is given by

$$U'_T = \begin{pmatrix} \exp(2i\Theta_s) & 0 & 0 & 0 \\ 0 & 1 & 0 & 0 \\ 0 & 0 & 1 & 0 \\ 0 & 0 & 0 & 1 \end{pmatrix}. \quad (\text{S35})$$

TABLE S1. Implementation examples of two-qubit geometric gates

| gate                 | matrix   | parameters<br>( $\Theta_s, \theta_0, \theta_1, \theta_2, \phi$ ) |
|----------------------|--|--|
| controlled-Not       | $\begin{pmatrix} 0 & 1 & 0 & 0 \\ 1 & 0 & 0 & 0 \\ 0 & 0 & 1 & 0 \\ 0 & 0 & 0 & 1 \end{pmatrix}$   | $(\pi/2, 0, \pi/2, \pi/2, \pi)$                                  |
| SWAP                 | $\begin{pmatrix} 1 & 0 & 0 & 0 \\ 0 & 0 & 1 & 0 \\ 0 & 1 & 0 & 0 \\ 0 & 0 & 0 & 1 \end{pmatrix}$   | $(\pi/2, -\pi/2, 0, \pi, \pi)$                                   |
| $\sqrt{\text{SWAP}}$ | $\begin{pmatrix} 1 & 0 & 0 & 0 \\ 0 & \frac{1}{2}(1+i) & \frac{1}{2}(1-i) & 0 \\ 0 & \frac{1}{2}(1-i) & \frac{1}{2}(1+i) & 0 \\ 0 & 0 & 0 & 1 \end{pmatrix}$ | $(\pi/4, -\pi/2, \pi, 0, \pi)$                                   |

In the computational subspace spanned by  $\{|\tilde{0}\rangle_a|\tilde{0}\rangle_b, |\tilde{0}\rangle_a|\tilde{1}\rangle_b, |\tilde{1}\rangle_a|\tilde{0}\rangle_b, |\tilde{1}\rangle_a|\tilde{1}\rangle_b\}$ , the evolution operator  $U'_T$  reads

$$U'_T(1 : 4, 1 : 2) = e^{i\Theta_s} \begin{pmatrix} e^{-i\Theta_s} + 2i \sin \Theta_s \cos^2 \frac{\theta_0}{2} \cos^2 \frac{\theta_1}{2} & \frac{i}{2} e^{-i\phi} \sin \Theta_s \sin \theta_1 (1 + \cos \theta_0) \\ \frac{i}{2} e^{i\phi} \sin \Theta_s \sin \theta_1 (1 + \cos \theta_0) & e^{-i\Theta_s} + 2i \sin \Theta_s \cos^2 \frac{\theta_0}{2} \sin^2 \frac{\theta_1}{2} \\ ie^{i\phi} \sin \Theta_s \sin \theta_0 \cos \frac{\theta_1}{2} \cos \frac{\theta_2}{2} & i \sin \Theta_s \sin \theta_0 \sin \frac{\theta_1}{2} \cos \frac{\theta_2}{2} \\ ie^{i\phi} \sin \Theta_s \sin \theta_0 \cos \frac{\theta_1}{2} \sin \frac{\theta_2}{2} & i \sin \Theta_s \sin \theta_0 \sin \frac{\theta_1}{2} \sin \frac{\theta_2}{2} \end{pmatrix},$$

$$U'_T(1 : 4, 3 : 4) = e^{i\Theta_s} \begin{pmatrix} ie^{-i\phi} \sin \Theta_s \sin \theta_0 \cos \frac{\theta_1}{2} \cos \frac{\theta_2}{2} & ie^{-i\phi} \sin \Theta_s \sin \theta_0 \cos \frac{\theta_1}{2} \sin \frac{\theta_2}{2} \\ i \sin \Theta_s \sin \theta_0 \sin \frac{\theta_1}{2} \cos \frac{\theta_2}{2} & i \sin \Theta_s \sin \theta_0 \sin \frac{\theta_1}{2} \sin \frac{\theta_2}{2} \\ e^{-i\Theta_s} + 2i \sin \Theta_s \sin^2 \frac{\theta_0}{2} \cos^2 \frac{\theta_2}{2} & \frac{i}{2} \sin \Theta_s \sin \theta_2 (1 - \cos \theta_0) \\ \frac{i}{2} \sin \Theta_s \sin \theta_2 (1 - \cos \theta_0) & e^{-i\Theta_s} + 2i \sin \Theta_s \sin^2 \frac{\theta_0}{2} \sin^2 \frac{\theta_2}{2} \end{pmatrix}, \quad (\text{S36})$$

which describes a universal two-qubit geometric gate (see Tab. S1 for examples). These two-qubit gates using the same strategy as the single-qubit case are also insensitive to the errors induced by pulse imperfections [see the purple-solid curve in Fig. S1(b)]. Therefore, when considering the error coefficient  $\delta_i = 0.1$ , in Fig. S1(c), we show that arbitrary two-qubit gates can be implemented with high fidelities.